Chapter 3

Verification

3.0 Concept and literature review

The increasing demand of CFD numerical codes in various scientific and engineering fields calls for methods to establish the accuracy of the numerical scheme. With increases in computational power, CFD practitioners often focus on solving more complex and difficult problems rather than demonstrating the accuracy of their current problems which can lead to a decrease in the quality of their simulations. Previous works on verification and validation in the CFD community [1-6] define verification as demonstrating the mathematical correctness of the numerical simulation. This usually means that if the observed discretization error decreases to zero as the mesh increments decrease to zero, then the equations are "solved correctly". In other words, code verification is a procedure to demonstrate that the governing equations, as implemented in the code, are solved consistently.

Verification of CFD codes has been the subject of many studies in recent years. Abanto et al [3] demonstrated an approach to test the accuracy of some of the most widespread commercial codes. They presented grid convergence studies on atypical CFD cases using some commercial CFD packages. Their verification test cases include an incompressible laminar Poiseuille flow, a manufactured incompressible laminar boundary layer flow, an incompressible re-circulating flow and an incompressible annular flow. Different types of structured and unstructured meshes were used during the study. They observed non-monotonic grid convergence for all their test cases. Iterative convergence of the discrete equations to machine zero did not guaranty accurate flow field predications which meant that the codes converged to wrong solutions. From their study, they recommended that users perform the

verification of commercial CFD codes and be cautious when using the commercial codes on industrial problems.

Kleb and Wood [4] pointed out that the computational simulation community is not routinely publishing independently verifiable tests to accompany new models or algorithms. They mentioned the importance of conducting component-level verification tests before attempting system-level verification and also publishing them when introducing a new component algorithm. They proposed a protocol for the introduction of new methods and physical models that would provide the computational community with a credible history of documented, repeatable verification tests that would enable independent replication.

Roache [1, 5] discussed the verification of codes and calculations along with some definitions and descriptions related to confidence building in computational fluid dynamics. Verification was described as solving the equations right and validation as solving the right equations. Different aspects discussed in the paper include the distinction between code verification and validation, grid convergence and iterative convergence, truncation error and discretization error. Also discussed were verification of calculations, error taxonomies, code verification via systematic grid convergence testing, the Grid Convergence Index (GCI) and sensitivity of grid convergence testing. According to the author, verification does not include all aspects of code quality assurance like the important concerns of version control or archiving of input data. In the books by Roache et al [5], the authors comprehensively discussed code verification, the Method of Manufactured Solutions (MMS) used to obtain exact solutions for code verification purposes, and order of accuracy verification.

A more recent study of code verification conducted by Shunn et al [6] demonstrates the MMS verification technique as applied to variable density solvers. In this study, verification was used to investigate the effects of tabulated state-equations and temporal iteration errors on the convergence and accuracy of the code. The two problems constructed were diffusive mixing of species, and convection of density fronts which reflect basic physical phenomena found in combustion problems. Grid refinement studies performed confirm the spatial convergence rate of solver to be second order when an analytical equation of state (EOS) is used. Convergence of the flow variables to the exact solution were found to be impaired when the EOS was linearly interpolated in space. It was also found that EOS interpolation errors introduce spurious numerical fluctuations in the flow variables, with velocity and pressure being particularly vulnerable. This particular variable density algorithm showed first order temporal evolution of the flow when a single outer density iteration was applied. Temporal errors were generally not dominant when multiple outer density iterations were performed, making it difficult to confirm the temporal accuracy of the method with multiple outer iterations.

3.1 Verification procedures

The intent of this chapter is to present a suitable verification framework that can be applied to our own in-house solver, les3d-mp. The procedure can be used to provide a pass-fail acceptance criteria commonly used in the community to establish the validity of cfd solvers [6]. This same procedure is found to be very helpful in detecting coding mistakes (bugs) that are associated with spatial or temporal discretization of the transport equations. The need for verification in this project arises due to the introduction of numerical schemes and models to account for variable density Low-Mach number physics. Numerical schemes and model developments were presented in chapter 2.

Currently, our verification procedure consists of comparing our computational solution to an exact analytical solution representative of the physics involved in low-mach number problems. Comparing to an exact solution is called MES, or method of exact solutions, and is a powerful verification technique when one can develop an analytical solution for a test case. Comparing to an exact solution brings up the notion of discretization errors which are inherent to any solver that discretizes a set of governing PDEs into a finite dimensional subspace which approximates the continuum solution. The difference between the two is the discretization error. Discretization methods are *consistent* if the error goes to zero as the representative cell size, h, decreases to zero (for mesh size h, then a consistent method will result in error that is proportional to h^p). The rate at which the error decreases to zero is called the order of accuracy. A discretization method is said to be second order accurate in space if the discretization error goes to zero as h^2. According to the community the most rigorous acceptance criterion is verification of order of accuracy, in which one not only seeks to verify that the method is consistent, but also establishes the value of p and is then compared to the theoretical order of the discretization method. This is our established procedure.

The following sections present spatial and temporal order of accuracy test cases that have been developed with variable density transport equations in mind. The first part presents cases related to spatial order of accuracy where we seek to establish the second order accuracy of the code through two test cases: a one dimensional isothermal binary mixing case and a two-dimensional solution of the poiseuille equations with variable density. We then seek to show the temporal order of accuracy through studies of time-periodic poiseuille solution and classical version of Stoke's 2nd problem where exact solutions are also presented. Lastly, classical boundary layer test cases corresponding to the free-convection and natural convection regime are presented establishing the fidelity of the solver in computing these canonical flows.

3.2 Spatial accuracy cases

3.2.1. Isothermal Binary Mixing

The following verification case tests the ability to handle flows with large density ratios similar to those found in fires or in combustion systems. An exact solution to the one dimensional mixing of two fluids with different molecular weights is presented. The mixing occurs at constant temperature and constant pressure conditions. Next, a measure of the global Discretization error is obtained on a series of different meshes and the error is computed on each mesh. This information yields the spatial order of accuracy of the code. If the discrete solution is second order in space, then the RMS error, $||L_2||$ will decrease by a factor of 4 for every halving of the grid cell size. In this case, the normalized global error is defined as:

$$\left|\left|L_2\right|\right| = \sqrt{\frac{1}{N}\sum\left(u_j - U_j\right)^2}$$

where u_j is the exact solution and U_j the discrete solution.

3.2.1.1 Governing Equations

An exact solution for the binary mixing problem is found for the density field which directly couples the mixture fraction scalar and lateral component of velocity. The solution has the characteristic of being a transient mass-density diffusion equation satisfying, $\frac{\partial \rho}{\partial t} = D\frac{\partial^2 \rho}{\partial y^2}$. The density field solution has the following form:

$$\rho(y,t) = \rho_2 + (\rho_1 - \rho_2)\frac{\delta_0}{\sqrt{4\pi D(t+t_0)}}e^{\frac{-y^2}{4D(t+t_0)}}$$

Where the density values are assigned through molecular weights of heavy and light fluids through an equation of state (EOS) and δ_0 represents a characteristic mixing length scale. The mixture fraction field for the first scalar is now defined as,

$$Z(y,t) = \frac{\frac{1}{\rho(y,t)} - \frac{1}{\rho_2}}{\frac{1}{\rho_1} - \frac{1}{\rho_2}}$$

Using the one-dimensional continuity equation with transient and lateral velocity terms gives the vertical component of velocity as,

$$v(y,t) = \frac{(\rho_1 - \rho_2)}{\rho(y,t)} \frac{\delta_0}{\sqrt{4\pi D(t+t_0)}} \left(\frac{y}{2(t+t_0)}\right) e^{\frac{-y^2}{4D(t+t_0)}}$$

It should be noted that all the above solutions have a singularity at time (*t =0*), thus an offset time,t_0, is added based on diffusion time scales to avoid an unphysical solution. The analysis of this problem begins at t_0=10. Also note that the reference density fields corresponding to isothermal light and heavy fluid mixing in air (ρ_1, ρ_2) are defined through the use of the equation of state (Table 1). The species fraction of oxygen and nitrogen in air are: $Y_{0_{2air}} =$ 02.33 and $Y_{N_{2air}} = 1 - Y_{0_{2air}}$ are utilized to calculate the molecular weight of the mixture (air),

$$MW_{mix} = \frac{1}{\left(\frac{Y_{0_2}}{MW_{0_2}} + \frac{Y_{N_2}}{MW_{N_2}}\right)}$$

$$\rho_1 = \frac{MW_{mix}}{MW_1}$$

$$\rho_2 = \frac{MW_{mix}}{MW_2}$$

The verification task begins by initializing the code with the above equations at an offset time, t_0=10. The domain is selected as *(Lx, Ly, Lz) = (10,30,5.0)* with double periodic conditions in *Lx* and *Lz*. Grid design procedures are followed in order to resolve the

characteristic mixing layer, this has a minimum length-scale of 2 and increases to 20 by the end of the simulation. Adequate resolution will ensure to have at least 30-40 points inside the minimum mixing layer set by the initial conditions. The running time is selected based on a parametric study of density ratios (Figure 1) where a peak density ratio value was found at initial offset time ($\frac{\rho_2}{\rho_1} = 19$) and decreased exponentially to nearly 1 at an approximate time of 400 time units. The density ratio values are graphically compared to the reference density field (ρ_1) showing that a running time of t = 100 captures the transient dynamics of interest. This is shown by the following figures where the history of peak density ratios are evaluated at the bottom of the domain.

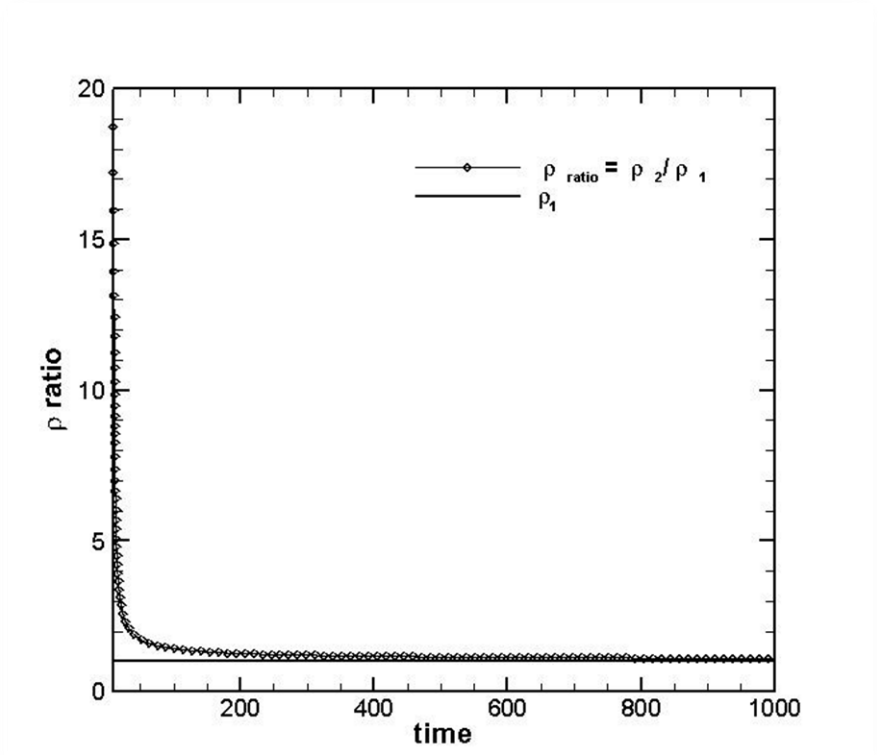

ν_{inf} *	$Pr = \frac{c_p \mu}{k}$	MW_{mix}	ρ_1^*	ρ_2^*
0.02	0.75	$\frac{1}{\left(\frac{Y_{O_2}}{MW_{O_2}} + \frac{Y_{N_2}}{MW_{N_2}}\right)}$	$\frac{MW_{mix}}{MW_1} = 0.0097$	$\frac{MW_{mix}}{MW_2} = 1$
	t_0 **(off-set time)**	δ_0 **(characteristic lengthscale)**	Re_{ref}	$T_{inf}(K)$
	10	2	50	300

$(L_x L_y L_z)^*$	$(n_x n_y n_z)$	***grid stretching***
(10,30,5)	(10,2400,4)	Uniform grid in x, z, y
Initial Conditions	**Specific Enthalpy model**	***farfield boundary***
$u_{init} = 0, w_{init} = 0$ $v_{init} = v_{exact}(t = t_0)$ $Z_{init} = Z_{exact}(t = t_0)$ $h_{init} = h^*(Z_{init}, T_{amb})$	Chemkin coefficient data base w/ enthalpy polynomial: $h^* = a_6 + a_1 T + \frac{c_2 T^2}{2} + \frac{c_3 T^3}{3} + \frac{c_4 T^4}{4} + \frac{c_5 T^5}{5}$	$u_{farfield} = 0$ $\frac{dv}{dy} = 0, \frac{dw}{dy} = 0$ $\frac{dh}{dy} = 0, \frac{dZ}{dy} = 0$
wall boundary	***Scalar Discretization Option***	***Periodicity***
$u_{i_{wall}} = No\ slip$ $T_{wall} = T_{inf}$	QUICK	Spanwise, Streamwise

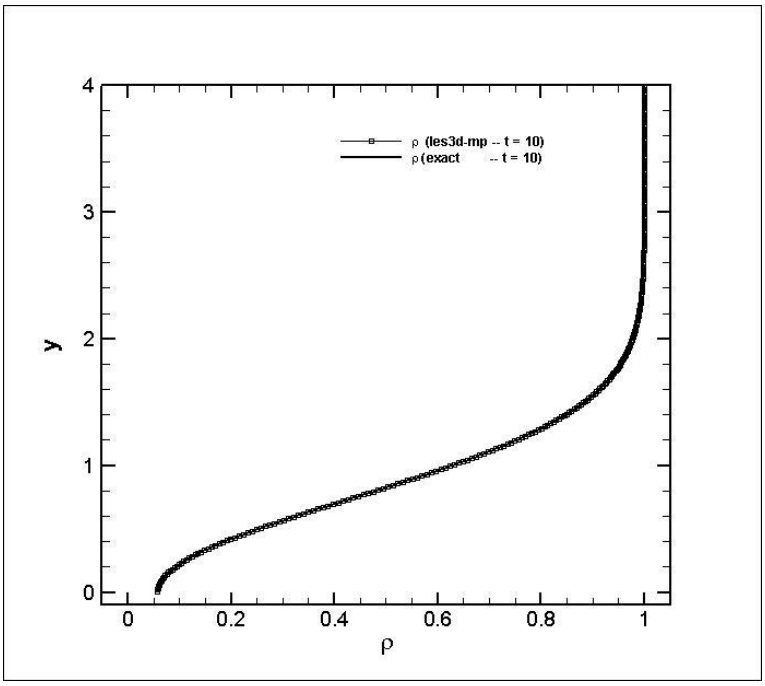
ρ (les3d-mp -- t = 10)
ρ (exact -- t = 10)
y
ρ
0
1
2
3
4
0
0.2
0.4
0.6
0.8
1

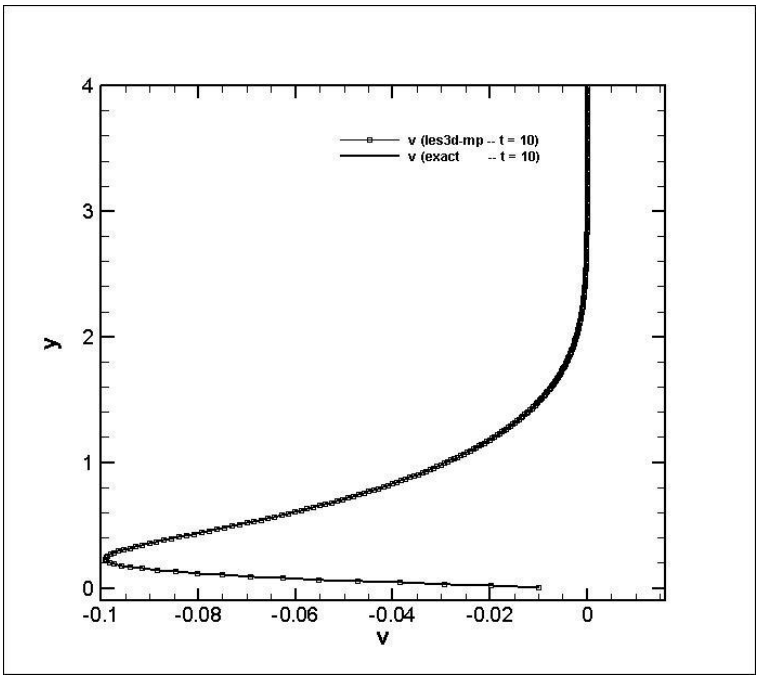
v (les3d-mp -- t = 10)
v (exact -- t = 10)
y
v
0
1
2
3
4
-0.1
-0.08
-0.06
-0.04
-0.02
0

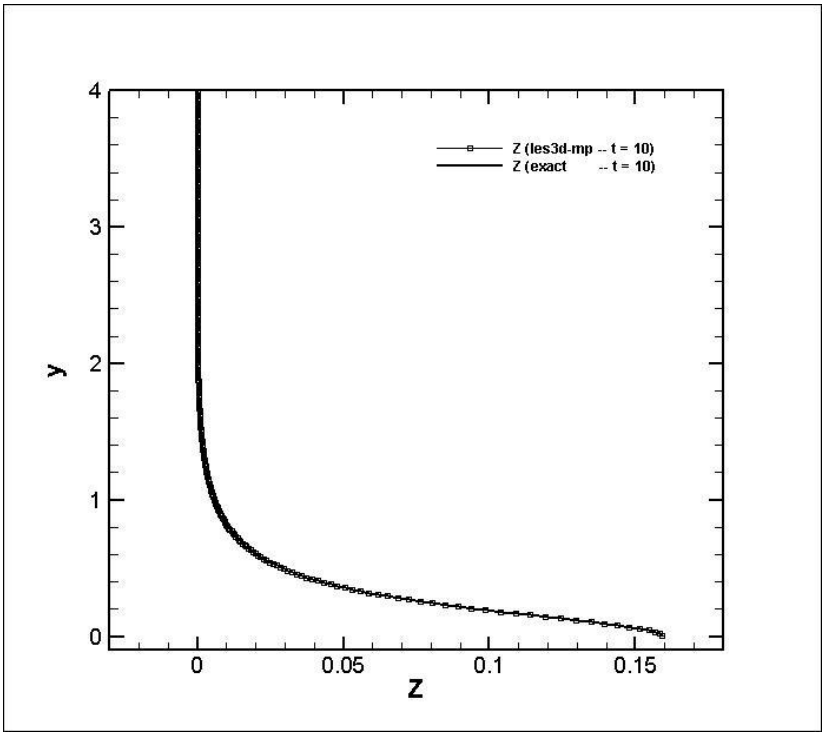
Z (les3d-mp -- t = 10)
Z (exact -- t = 10)
y
Z
0
1
2
3
4
0
0.05
0.1
0.15

3.2.1. Variable density Poiseuille Flow

Next, a formulation that accounts for the effects of variable density is presented. This is a spatially periodic flow solution that mimics an infinitely long channel in the streamwise direction. The addition of heat transfer and changes in the density field introduces an extra spatial dimensionality making this a 2D flow.

Table 1. Variable density parameter values.

Re	**Pra**	**LxLyLz**	**nxnynz**	**Periodicity**
50	1.0			x, z
$\boldsymbol{\mu}$	$\boldsymbol{c_p}$	$\boldsymbol{k}$	$\boldsymbol{T/T_w}$	**Scalar Scheme**
constant	constant	constant	2.0	QUICK

3.3 Temporal accuracy cases

This section deals with showing the order of accuracy of the time integrator in les3d-mp. Two time integrating options are available, they are second order Adams-Bashford and a third order, low-storage Runge Kutta scheme presented in section 2. A simple transient problem strictly defined as a function of time only, *f(t)* is selected in order to remove spatial errors from analysis. This takes the form of,

$$\frac{\partial u}{\partial t} = -sin(\omega t)$$

Where $\omega = \frac{2\pi}{T}$ and with the following initial condition, $u(0) = 0$. Since this test case is independent of spatial variables it can be run on a very coarse computational grid, such as (nx,ny,nz) = (4,4,4), or 4^3 and with a Reynolds number = 1. It makes use of periodic conditions in spanwise and streamwise directions as well as velocity symmetry conditions on the top and bottom boundaries. Symmetrical conditions are defined as zero wall-normal Neumann gradients in u & w velocities and zero Dirichlet lateral velocity at the boundaries of interest.

The velocity oscillation is introduced to les3d-mp by advancing the mean pressure gradient in time as the right hand side of the integrated solution. It is described through the mean pressure equation, $\frac{\partial \overline{P}}{\partial x} = -A\ sin\left(\frac{2\pi t}{T}\right)$, where the pressure gradient amplitude, A, and the wave period are given on Table 1. This transient ODE has the following analytical solution that is helpful in performing temporal order of accuracy studies,

$$u(t) = \frac{T}{2\pi}\big(1 - cos(\omega t)\big)$$

Table 2. Parameter values for transient test case.

parameter	value
T	10
A	1
Re	1
nxnynz	4x4x4
Periodicity	x, z

Running an order or accuracy analysis for a total running time of 3T/2 with increasingly finer time-steps (order of magnitude 10) gives the following results.

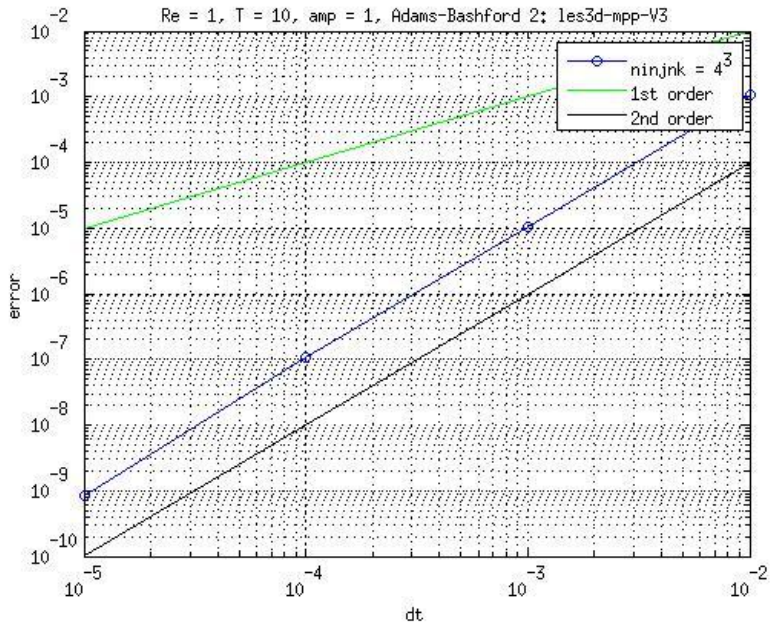

Establishing the 2nd order accuracy of the Adams-Bashford scheme.

3.3.1 Time-periodic Poiseuille flow

Table 3. Time-periodic parameter values.

Re	Pra	LxLyLz	nxnynz	Periodicity
50	1.0			x, z
μ	c_p	k	T/T_w	Scalar Scheme
constant	constant	constant	2.0	QUICK

3.3.2 Stoke's 2nd problem

Table 4. Stoke's 2nd problem parameter values.

Re	Pra	LxLyLz	nxnynz	Periodicity
50	1.0			x, z
μ	c_p	k	T/T_w	Scalar Scheme
constant	constant	constant	2.0	QUICK

3.4 Classical boundary layer solutions

3.4.1 Forced convection boundary layer: Blasius Solution

We now focus our attention to performing trend and expert judgment analysis of the canonical forced convection Blasius test case. Physically this is an important test case since it captures some of the salient features (i.e, wall shear stress, skin friction) found in momentum-driven boundary layers. Numerically this is also a challenging flow since it requires the implementation of inflow and outflow conditions to capture the spatially developing nature of the problem. The parameters necessary to implement this run are presented on Table 1 and results are shown for representative cases that correspond to the amount of heat transfer added as part of the simulation.

3.4.1.1 Results

The Blasius test cases have the following descriptions: Reynolds number of 50 with a displacement thickness and velocity of unity chosen as the reference length and velocity scales. It is performed on a computational domain of (Lx, Ly, Lz) = (200, 60, 5.0) having a total of 50,000 grid cells that spatially resolve the boundary layer. Standard grid design procedures are followed ensuring that 30-40 points are used to resolve the boundary layer viscous region. This is achieved through grid stretching by means of a hyperbolic tangent function which clusters the grids near the wall. This capability allows us to be more efficient in resolving the boundary layer thickness, δ.

Testing Parameters

$\boldsymbol{\nu_{inf}(m/s^2)}$	$\boldsymbol{Pr = \frac{c_p \mu}{k}}$	$\boldsymbol{T_{wall}, T_{inf}(K)}$	$\boldsymbol{\nu_{wall}\ (m/s^2)}$	$\boldsymbol{k_{inf}(m/s^2)}$
0.02	0.71	$450, 30K$	$\nu_{inf}\left(T_w/T_a\right)^{1.6} = 0.0383$	$\frac{c_p \nu_{inf} \rho_{inf}}{Pr} = 0.0539$
$\boldsymbol{L_0 - L_z}$	$\boldsymbol{Re_x}$	$\boldsymbol{\delta^*(z = L_0)\ (m)}$ *(displacement thickness)*	$\boldsymbol{\delta(z = L_0)\ (m)}$ *(boundary layer thickness)*	
$16.84\ - 200\ m$	842-10,000	1	3	
$\boldsymbol{U_{ref}\left(\frac{m}{s}\right)}$	$\boldsymbol{L_{ref} = \delta^*\ (m)}$	$\boldsymbol{\nu_{ref}\left(\frac{m}{s^2}\right)}$	$\boldsymbol{Re_{ref} = \frac{u_{ref} L_{ref}}{\nu_{ref}}}$	
1.0	1.0	0.02	50	

$\boldsymbol{(L_x L_y L_z)^*}$	$\boldsymbol{(n_x n_y n_z)}$	***grid stretching***	
(200,60,4)	(128,96,4)	- Wall –normal hyperbolic (α= 2.75) - Uniform grid in x, z	
Inflow boundary	***outflow boundary***	***freestream boundary***	
$u = u_{blasius}$, $v = v_{blasius}$, $w = 0$ $T = T_{wall}$	*Orlansky* $\frac{\partial u_i}{\partial t} + U_c \frac{\partial u_i}{\partial x_i} = 0$ $\frac{\partial h}{\partial t} + U_c \frac{\partial h}{\partial x_i} = 0$ $U_c = \frac{1}{L_y} \int u_{outflow} dy$	$\frac{du_i}{dy} = 0$ $\frac{dh}{dy} = 0$	*(Option)* $\frac{du}{dy} = 0, \frac{dw}{dy} = 0$ $v = v_{blasius}$ $\frac{dh}{dy} = 0$
wall boundary	***Scalar Discretization Optic***	***Periodicity***	
$u_{i_{wall}} = No\ slip$ $T_{wall} = 450K$	QUICK	Spanwise	

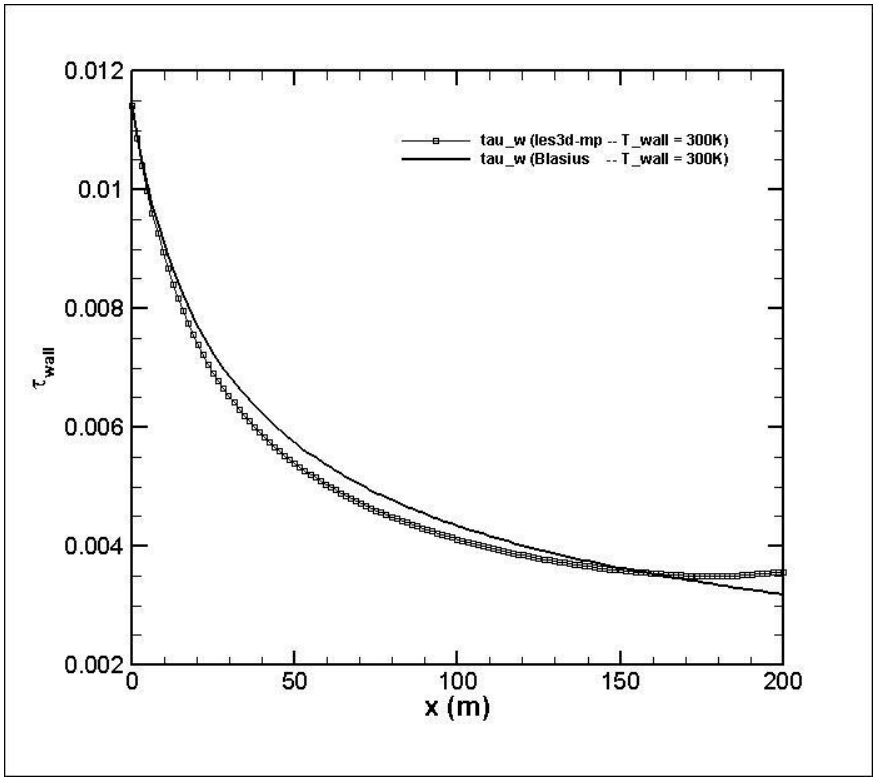
tau_w (les3d-mp -- T_wall = 300K)
tau_w (Blasius -- T_wall = 300K)
0.012
0.01
0.008
0.006
0.004
0.002
τwall
0
50
100
150
200
x (m)

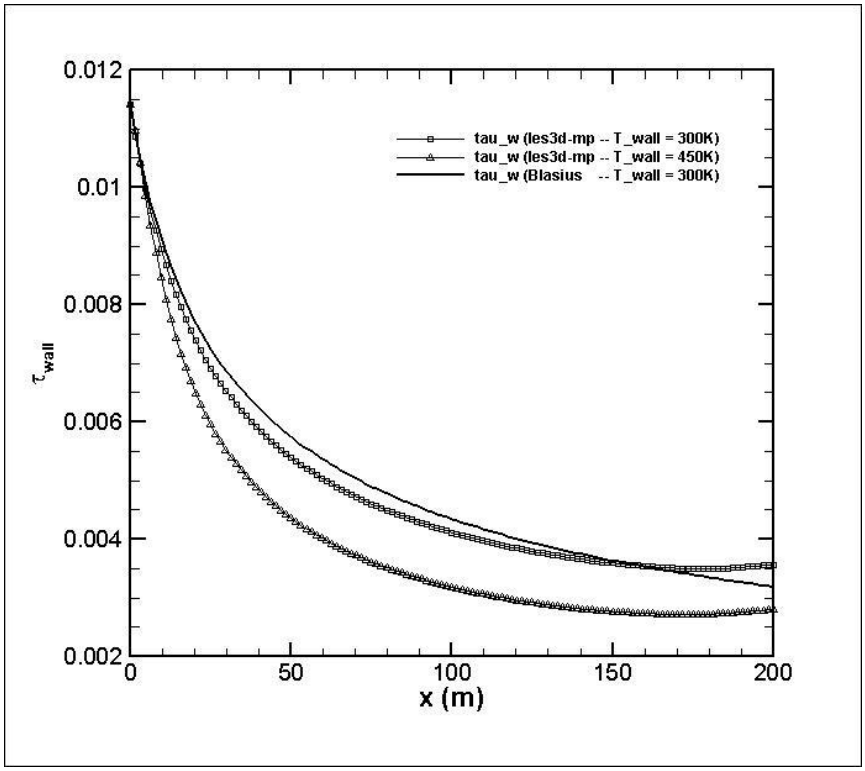
tau_w (les3d-mp -- T_wall = 300K)
tau_w (les3d-mp -- T_wall = 450K)
tau_w (Blasius -- T_wall = 300K)
0.012
0.01
0.008
0.006
0.004
0.002
τwall
0
50
100
150
200
x (m)

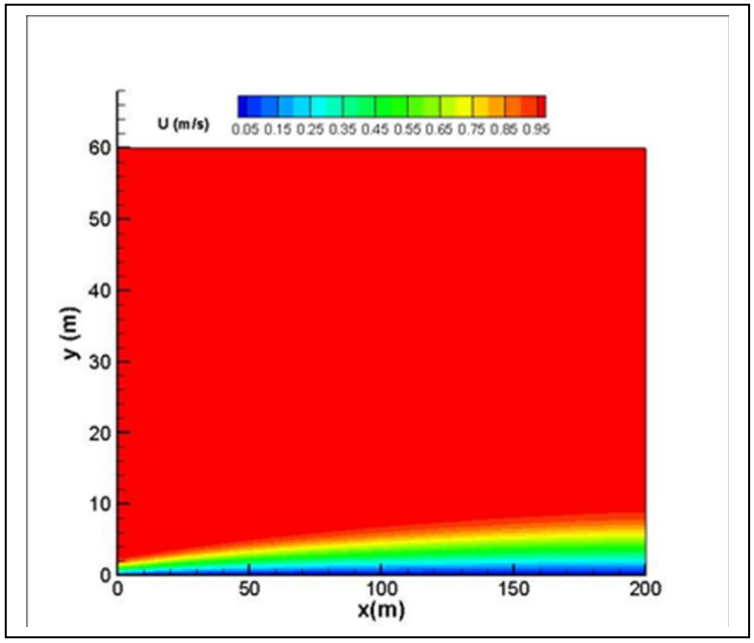
U (m/s)
0.05 0.15 0.25 0.35 0.45 0.55 0.65 0.75 0.85 0.95
y (m)
x(m)
0
10
20
30
40
50
60
0
50
100
150
200

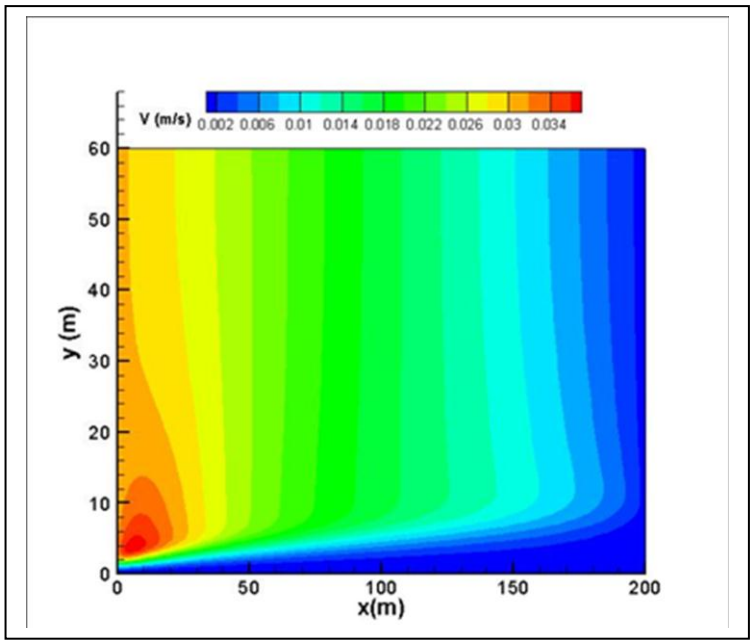
V (m/s)
0.002 0.006 0.01 0.014 0.018 0.022 0.026 0.03 0.034
y (m)
x(m)
0
10
20
30
40
50
60
0
50
100
150
200

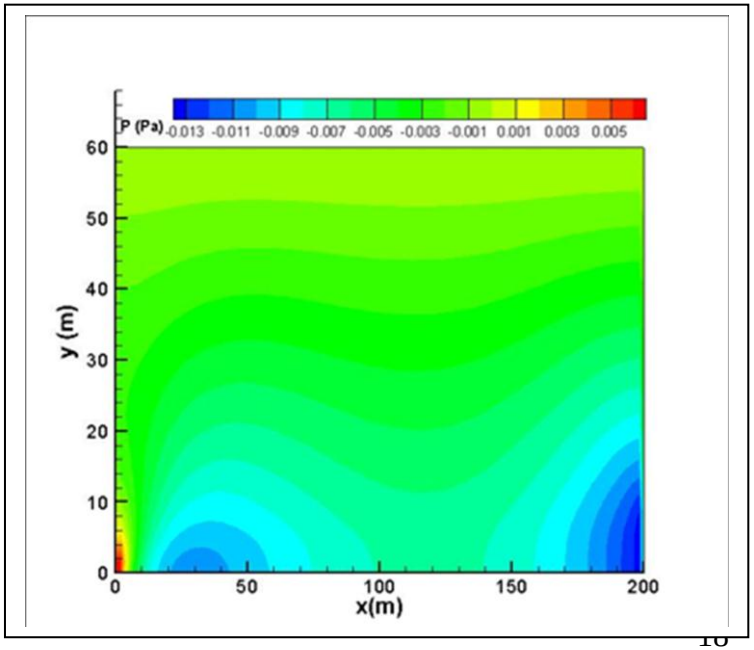
P (Pa)
-0.013 -0.011 -0.009 -0.007 -0.005 -0.003 -0.001 0.001 0.003 0.005
y (m)
x(m)
0
10
20
30
40
50
60
0
50
100
150
200

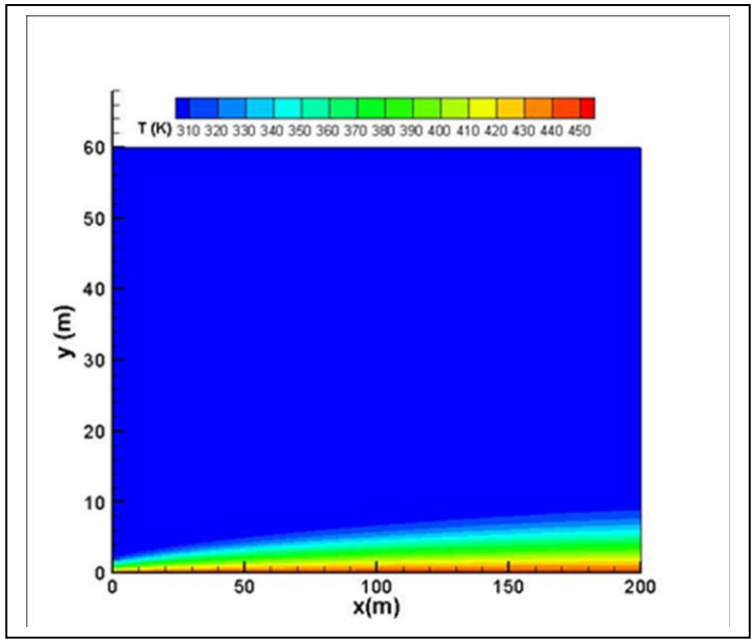
T (K)
310 320 330 340 350 360 370 380 390 400 410 420 430 440 450
y (m)
x(m)
0
10
20
30
40
50
60
0
50
100
150
200

3.4.2 Natural convection boundary layer: Ostrach Solution

The solution of laminar free convection boundary layer next to a heated isothermal plate was derived and developed by Ostrach [8]. This analysis presents a quasi-analytical solution to the posed problem based on similarity arguments and coupling between the temperature and velocity fields. Similar to the Blasius test case, velocity and temperature profiles are specified in order to provide a continuous inflow boundary condition. This allows control over the scaling of the solution since we can impose inflow conditions from our solution to the theoretical problem. An added difficulty in modeling flows in the free-convective regime is the introduction of an entrainment velocity. This lateral velocity is a salient feature of free-convective flow and is important in predicting the right amount of mixing and boundary layer growth.

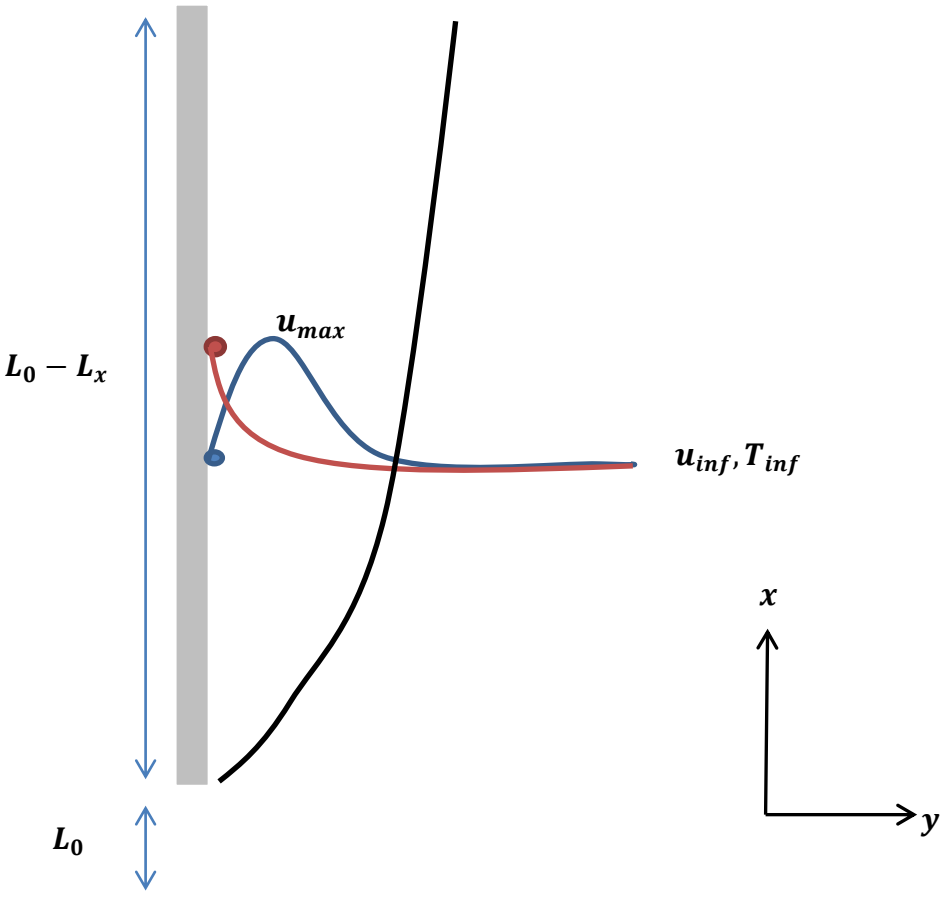

Testing parameters

$\nu_{inf}(m/s^2)$	$Pr = \frac{c_p \mu}{k}$	T_{wall}, T_{inf}	$\nu_{wall}\ (m/s^2)$	$k_{inf}(m/s^2)$
0.02	0.71	$360K, 300K$	$\nu_{inf}\left({}^{T_w}/_{T_a}\right)^2 = 0.0288$	$\frac{c_p \nu_{inf} \rho_{inf}}{Pr} = 0.0281$
$L_0 - L_z$	Gr_x	$\delta(x = 2m)\ (m)$	$U_{max}(x = 2m)\ \left(\frac{m}{s}\right)$	$U_{char}(x = 2m)\ ({}^{m}/_{s})$
$0.016\ m$ $- 20.0\ m$	$5.5E+01$ $- 6.9E+04$	1	1.1	$(g\beta\delta T L_z)^{0.5} = 1.97$
$U_{ref}\left(\frac{m}{s}\right)$	$L_{ref}\ (m)$	$\nu_{ref}\left(\frac{m}{s^2}\right)$	$Re_{ref} = \frac{u_{ref} L_{ref}}{\nu_{ref}}$	$Froude = g\left(\frac{L_{ref}}{U_{ref}^2}\right)$
1.1	2.0	0.02	110	16.2

$(L_x L_y L_z)^*$	$(n_x n_y n_z)$	***grid stretching***
(10,10,4)	(100,60,4)	- Wall –normal hyperbolic (α= 2.75) - Uniform grid in x, z
Inflow boundary	***outflow boundary***	***freestream boundary***
$u = 0.05, T = T_{inf}$ $\frac{dv}{dx} = 0, \frac{dw}{dx} = 0$	$Orlansky$ $\frac{\partial u_i}{\partial t} + U_c \frac{\partial u_i}{\partial x} - (\rho - \rho_\infty) g = 0$ $\frac{\partial h}{\partial t} + U_c \frac{\partial h}{\partial x} - (\rho - \rho_\infty) g = 0$	$\frac{du_i}{dy} = 0$ $\frac{dh}{dy} = 0$
wall boundary	***Scalar Discretization Option***	***Periodicity***
$u_{wall} = No\ slip$ $T_{wall} = 360K$	QUICK	Spanwise

Heat Flux

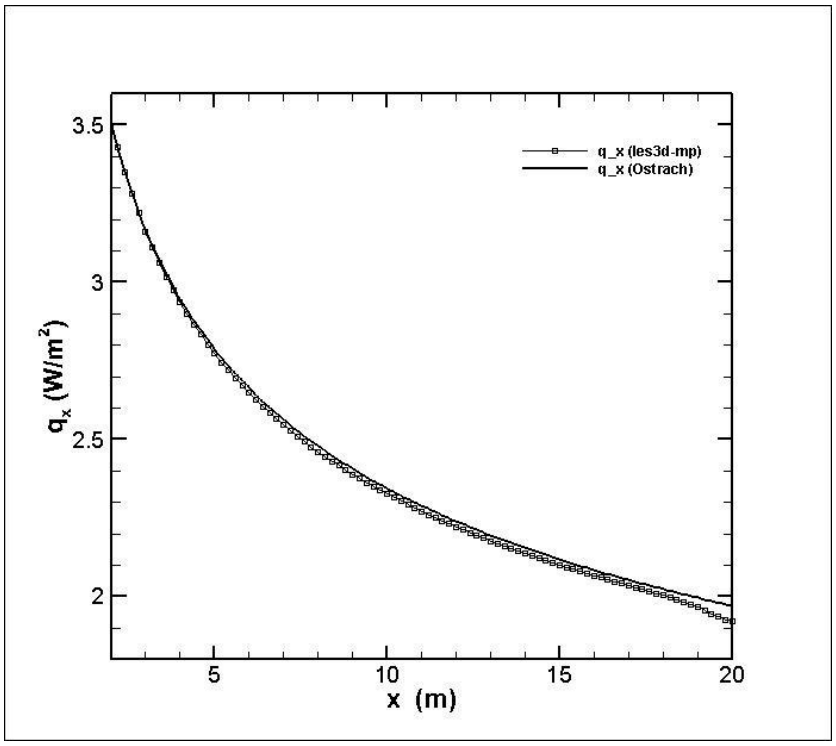
q_x (les3d-mp)
q_x (Ostrach)
3.5
3
2.5
2
q_x (W/m^2)
5
10
15
20
x (m)

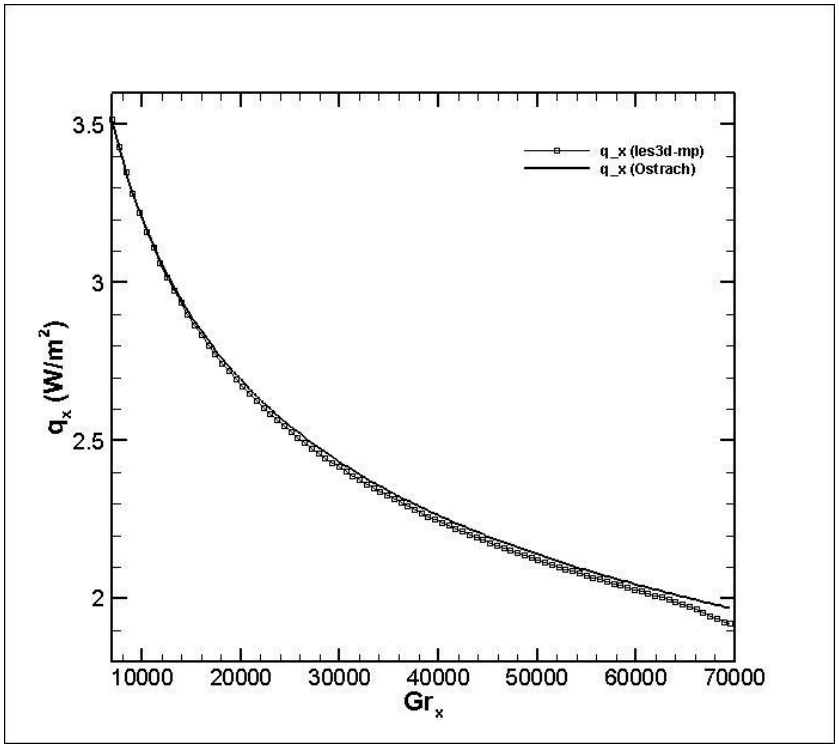
q_x (les3d-mp)
q_x (Ostrach)
3.5
3
2.5
2
q_x (W/m^2)
10000
20000
30000
40000
50000
60000
70000
Gr_x

Nusselt

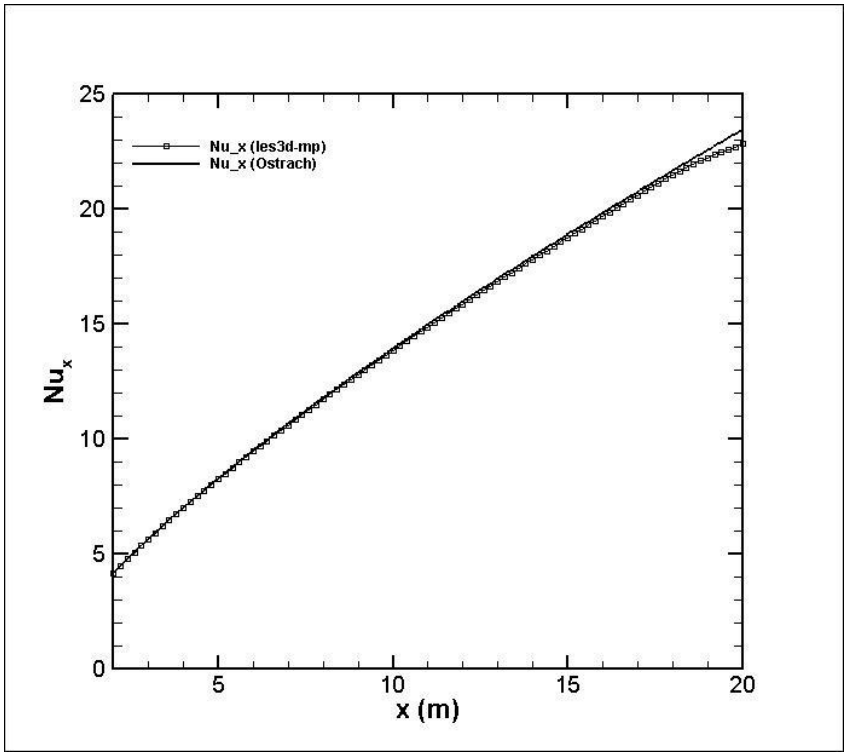
Nu_x (les3d-mp)
Nu_x (Ostrach)
Nu_x
x (m)
0
5
10
15
20
25

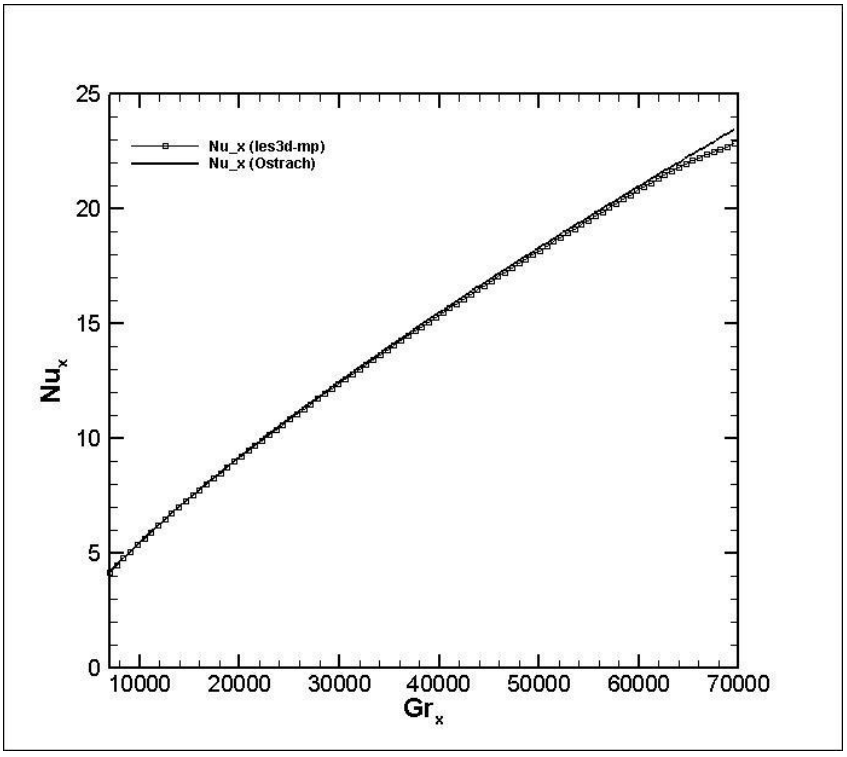
Nu_x (les3d-mp)
Nu_x (Ostrach)
Nu_x
Gr_x
0
5
10
15
20
25
10000
20000
30000
40000
50000
60000
70000

Time history of Pressure

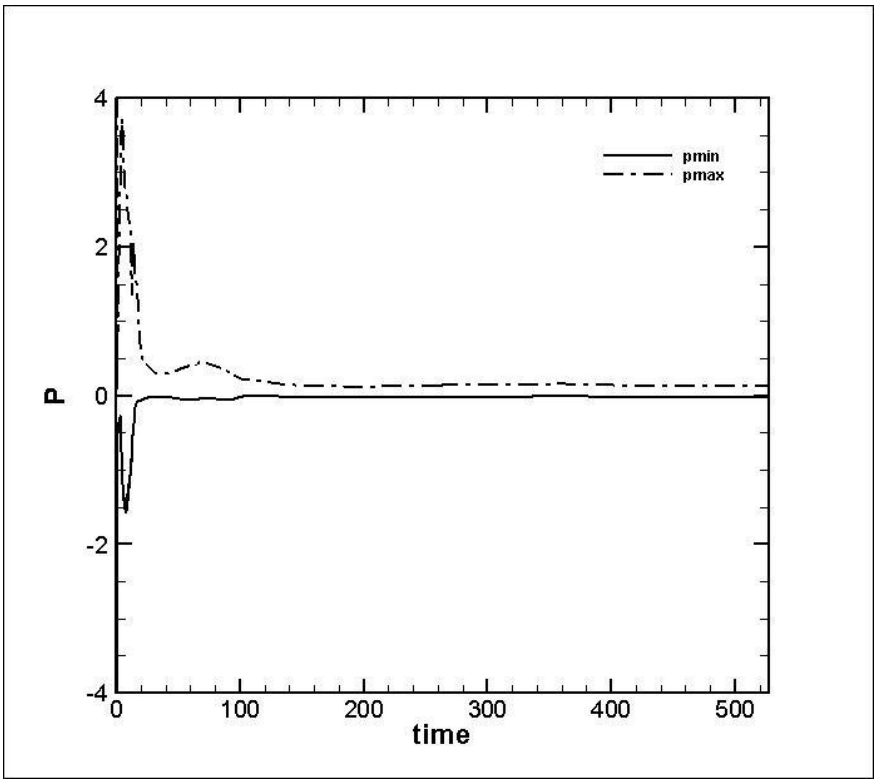

Velocity Profiles

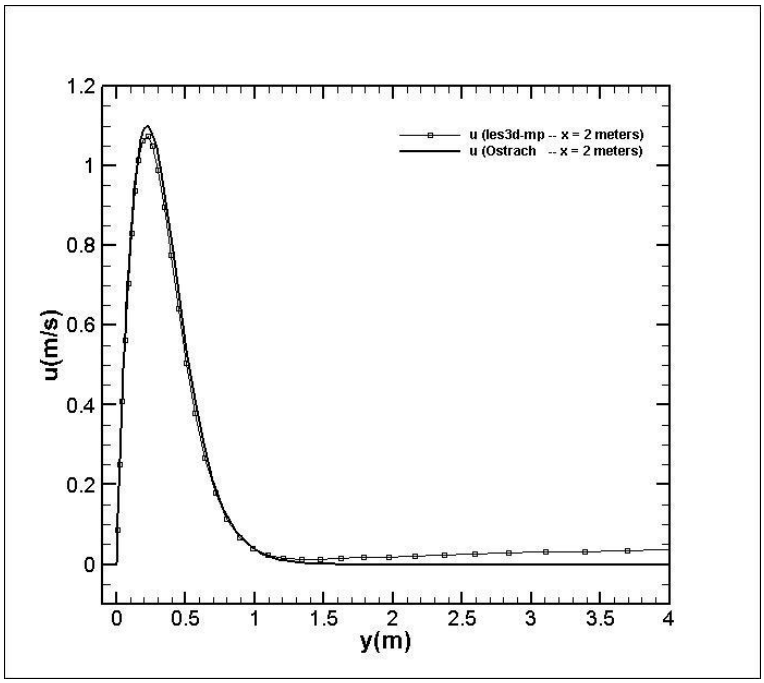

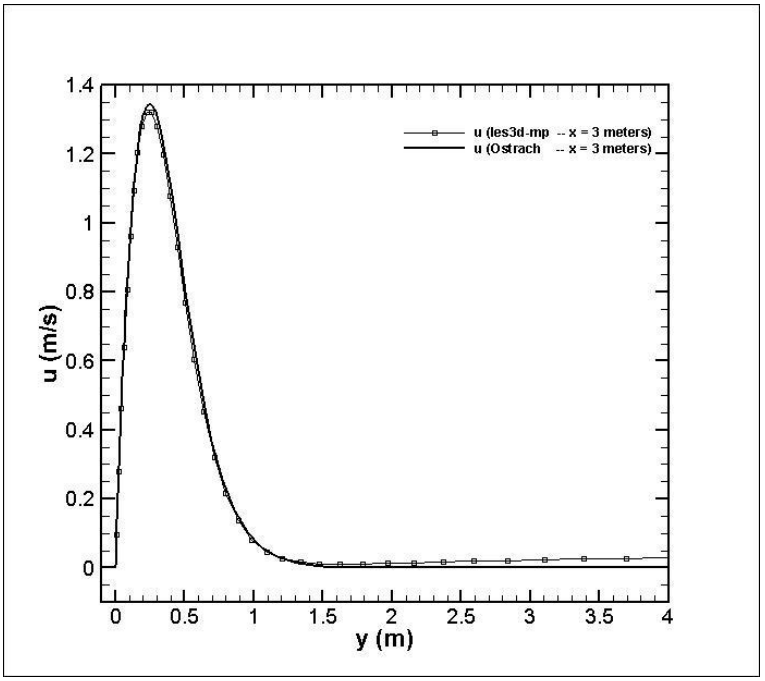

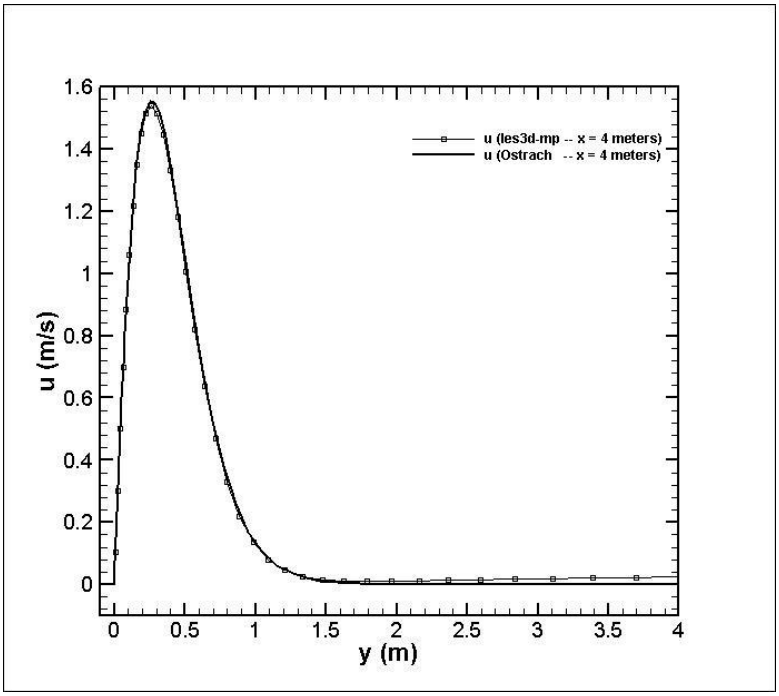

Temperature Profiles

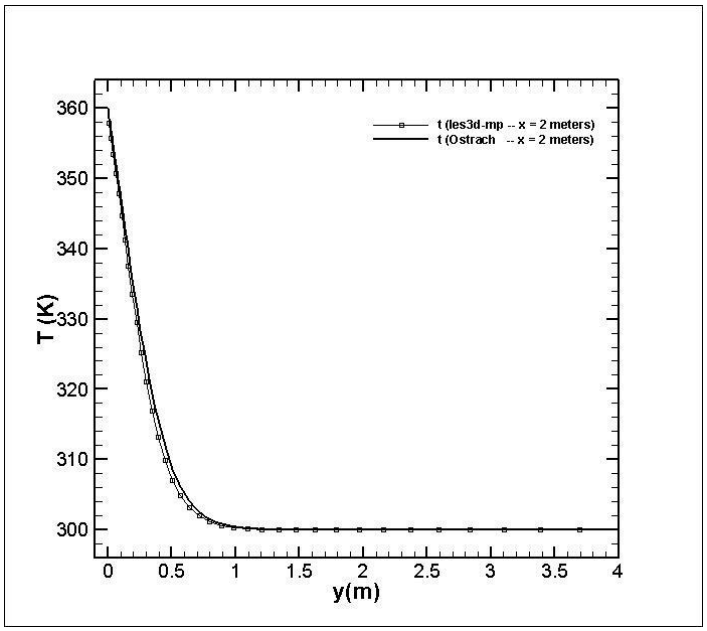

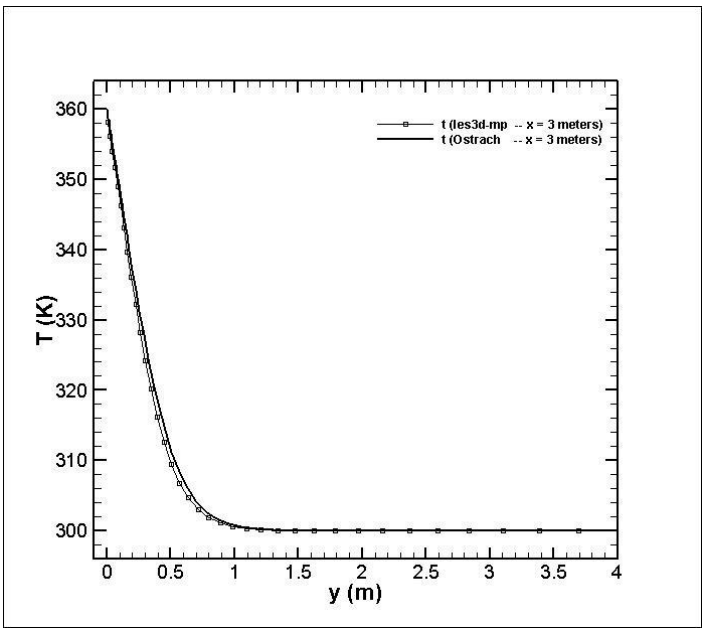

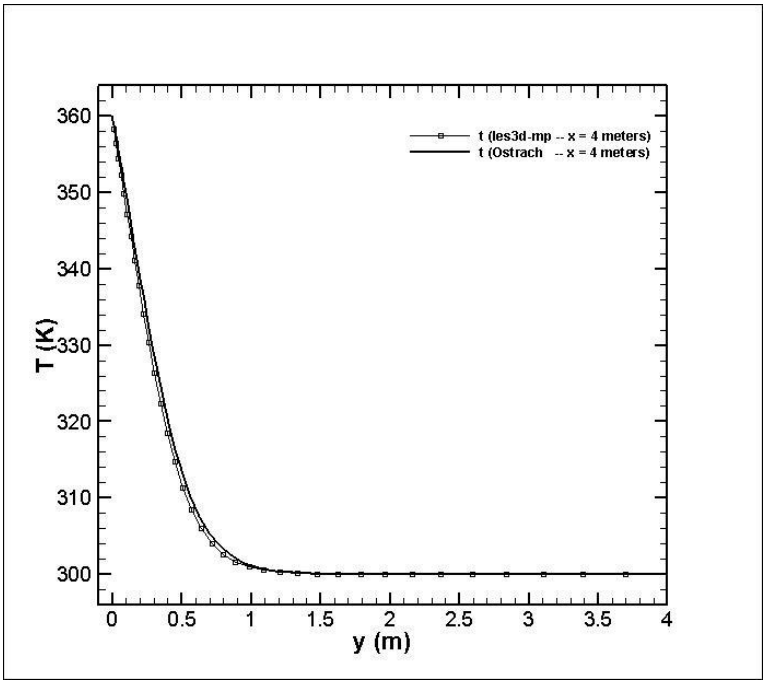

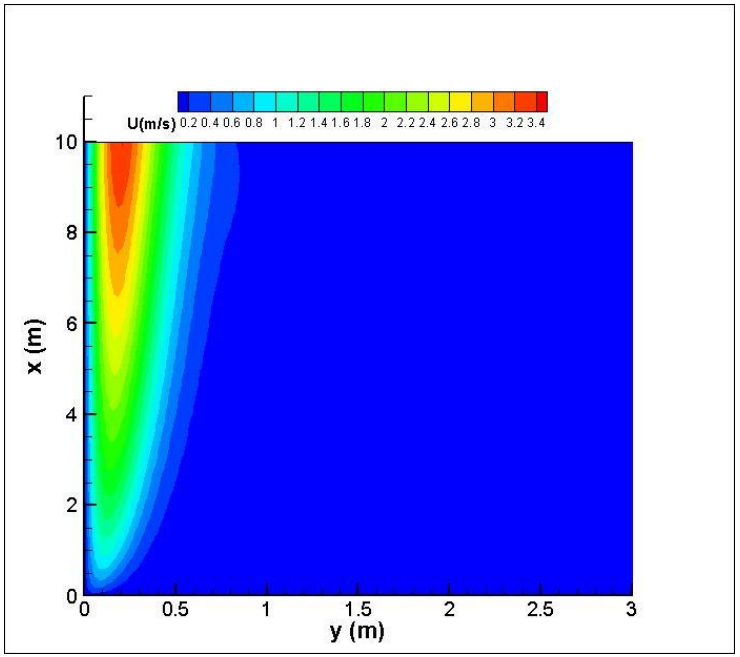
U(m/s) 0.2 0.4 0.6 0.8 1 1.2 1.4 1.6 1.8 2 2.2 2.4 2.6 2.8 3 3.2 3.4
x (m)
y (m)

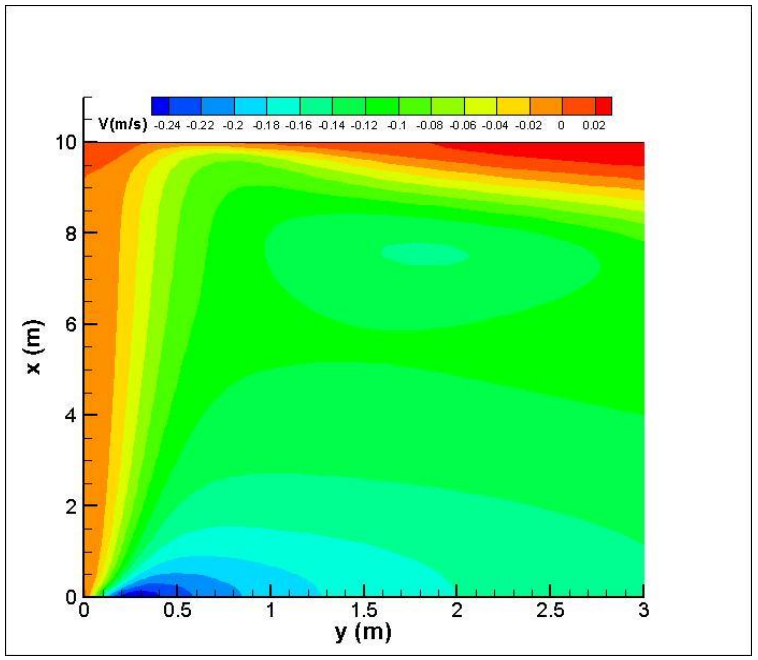
V(m/s) -0.24 -0.22 -0.2 -0.18 -0.16 -0.14 -0.12 -0.1 -0.08 -0.06 -0.04 -0.02 0 0.02
x (m)
y (m)

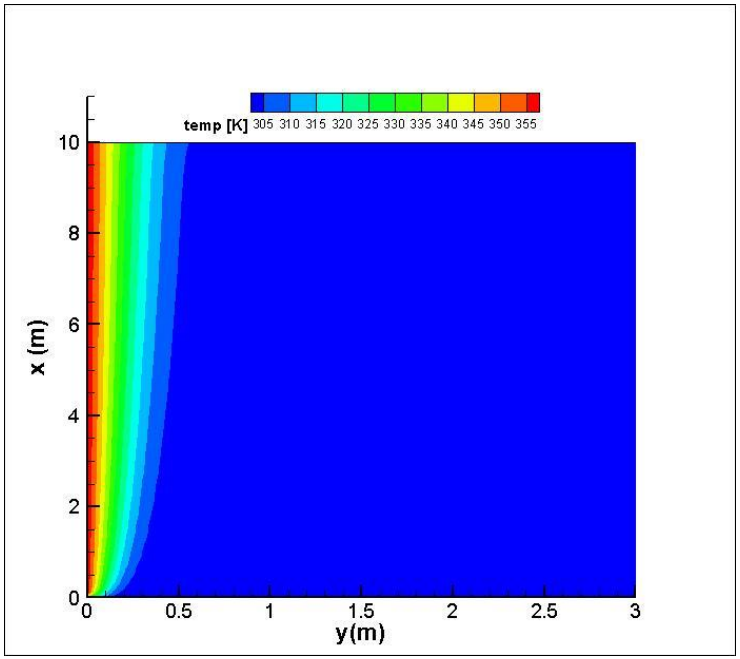
temp [K] 305 310 315 320 325 330 335 340 345 350 355
x (m)
y(m)

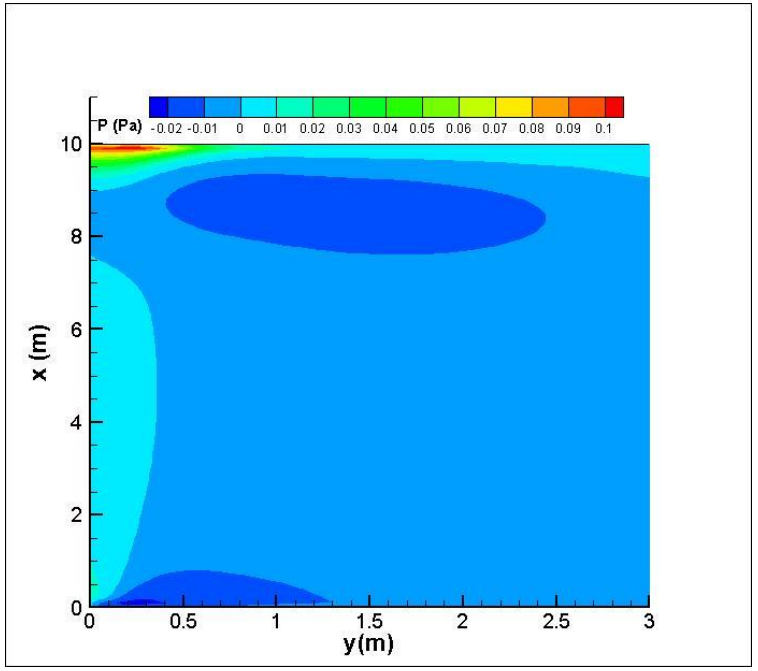
P (Pa) -0.02 -0.01 0 0.01 0.02 0.03 0.04 0.05 0.06 0.07 0.08 0.09 0.1
x (m)
y(m)

Reference

[1] P. J. Roache, Verification and Validation in Computational Science and Engineering, Hermosa Publishers, Albuquerque NM, 1998.

[2] "Guide for the Verification and Validation of Computational Fluid Dynamics Simulations," AIAA G-077-1998.

[3] Abanto, J., Pelletier, D., Garon, A., Trepanier, J. and Reggio, M., "Verification of some Commercial CFD Codes on Atypical CFD Problems," AIAA-2005-682, 43rd AIAA Fluid Dynamics Conference and Exhibit, January 2005.

[4] Kleb, B. and Wood, B., "CFD: A Castle in the Sand?," AIAA-2004-2627, 36th AIAA Fluid Dynamics Conference and Exhibit, June 2004.

[5] Roache, P. J., "Verification of Codes and Calculations," *AIAA Journal*, Vol. 36, No. 5, May 1998, pp. 696-702.

[6] Shunn, L., Ham, F., "Method of Manufactured Solutions Applied to Variable Density flow Solvers", Center for Turbulence Research Annual Briefs, 2007, pg 155-168.

[7] Orlansky, I; "A simple boundary condition for unbounded hyperbolic flows", *Journal of Computational Physics, **21**, 1976, pg 251.*

[8] Crawford, K; "Convective Heat and Mass Transfer", Textbook.